

Supplementary information

Antimony doping to greatly enhance the electrocatalytic performance of $\text{Sr}_2\text{Fe}_{1.5}\text{Mo}_{0.5}\text{O}_{6-\delta}$ perovskite as ceramic anode for solid oxide fuel cell

Shaowei Zhang,^a Kang Zhu,^a Xueyu Hu,^a Ranran Peng^a and Changrong Xia^{*ab}

^a CAS Key Laboratory of Materials for Energy Conversion, Department of Materials Science and Engineering, University of Science and Technology of China, No. 96 Jinzhai Road, Hefei, Anhui Province, 230026, P. R. China. E-mail: xiacr@ustc.edu.cn

^b Energy materials center, Anhui Estone Materials Technology Co. Ltd, 2-A-1, No.106, Chuangxin Avenue, Hefei, Anhui Province, 230088, P.R. China.

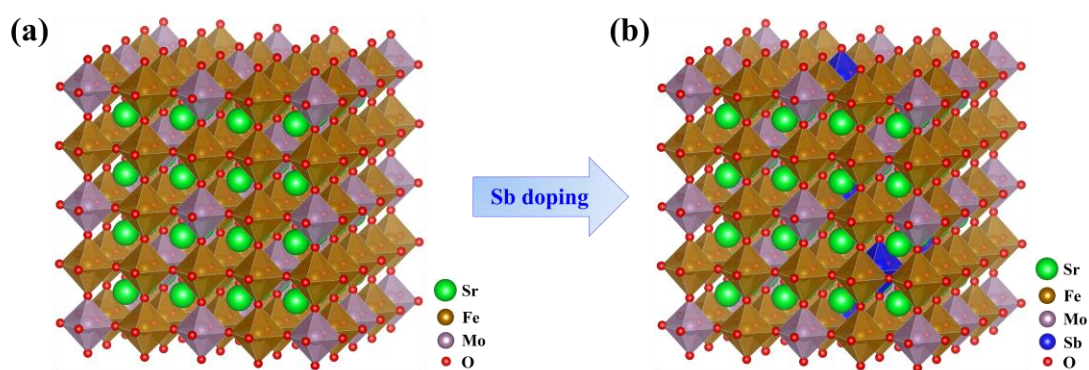


Fig. S1 Geometry structures for (a) SFM and (b) Sb-SFM. The supercell composition was set to $\text{Sr}_{64}\text{Fe}_{48}\text{Mo}_{16}\text{O}_{192}$ and $\text{Sr}_{64}\text{Fe}_{48}\text{Mo}_{12}\text{Sb}_4\text{O}_{192}$ with 320 atoms, which can be simplified as $\text{Sr}_2\text{Fe}_{1.5}\text{Mo}_{0.5}\text{O}_6$ and $\text{Sr}_2\text{Fe}_{1.5}\text{Mo}_{0.375}\text{Sb}_{0.125}\text{O}_6$, respectively.

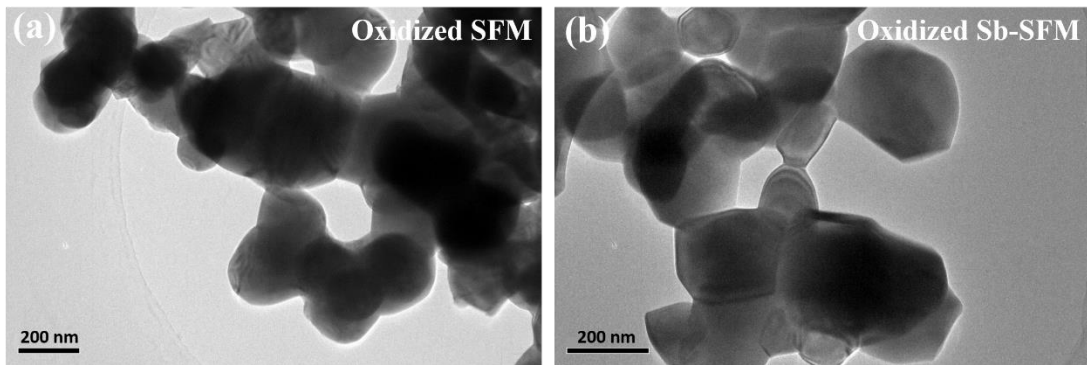


Fig. S2 TEM images for (a) oxidized SFM and (b) oxidized Sb-SFM powders. The crystal grains are connected to each other to form aggregated powders. The grain size is in the range of about 100-500 nm. Sb doping does not change the grain size and morphology.

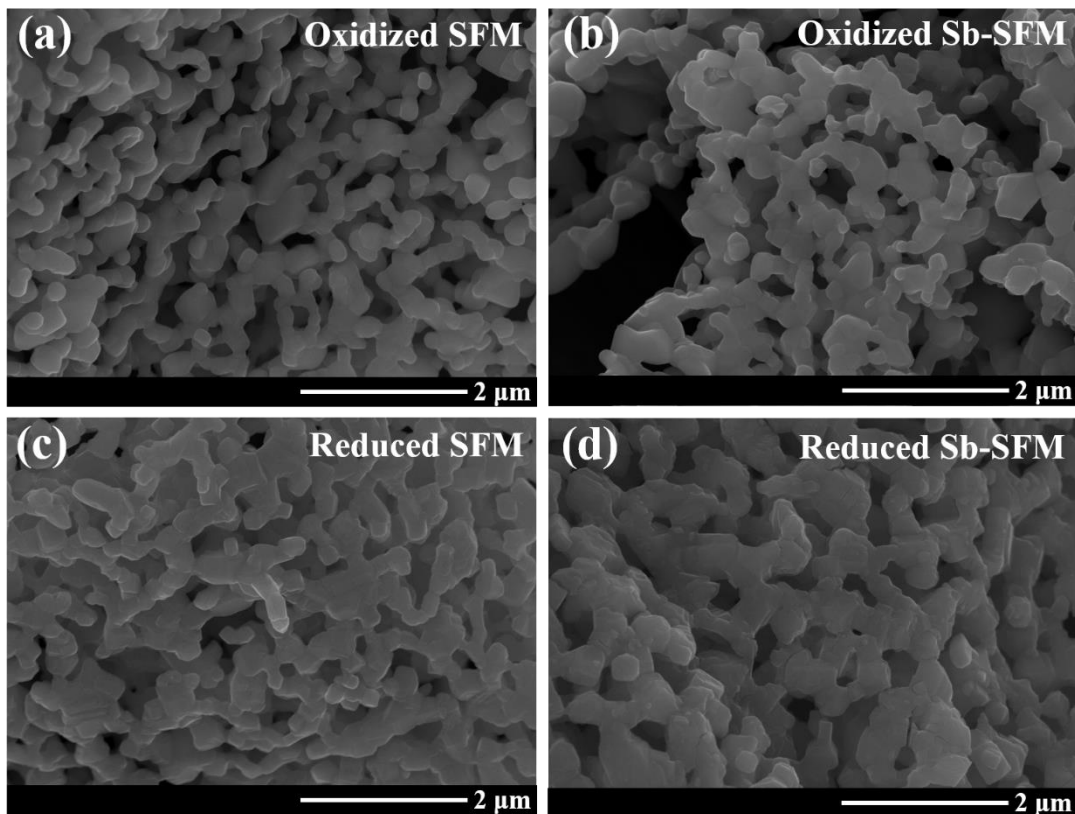


Fig. S3 SEM micrographs for SFM and Sb-SFM powders before and after reduction treatment in humidified H_2 at 800 °C for 5 h. (a) oxidized SFM, (b) oxidized Sb-SFM, (c) reduced SFM, and (d) reduced Sb-SFM. All the powders show almost the same microstructures, suggesting that Sb doping and reduction have negligible effects on the microstructures.

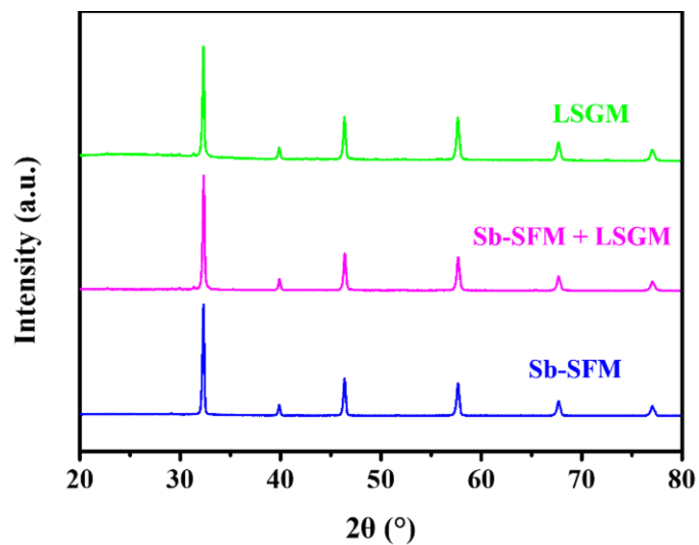


Fig. S4 XRD patterns for Sb-SFM, LSGM, and Sb-SFM~LSGM composite. The composite is obtained by heating Sb-SFM and LSGM mixture with a mass ratio of 1: 1 in air at 1100 °C for 2 h.

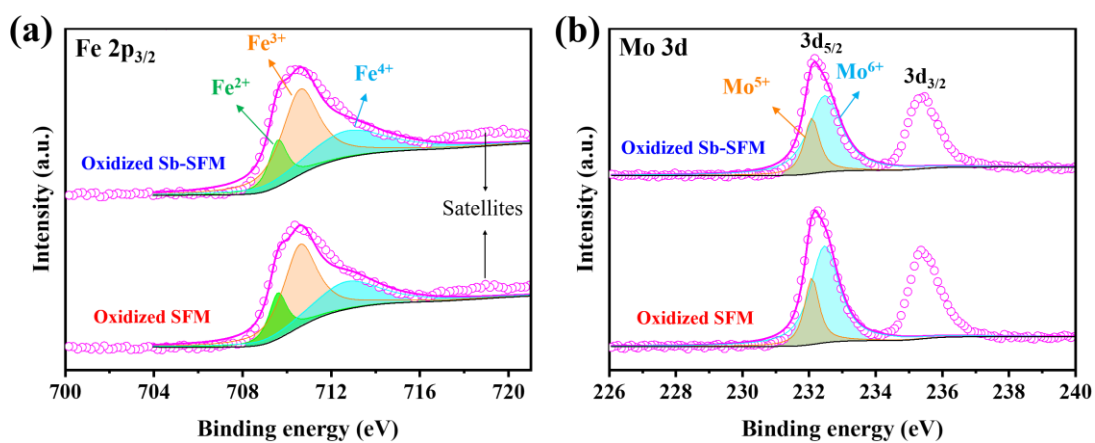


Fig. S5 XPS spectra for the oxidized SFM and Sb-SFM: (a) Fe 2p_{3/2}, (b) Mo 3d_{5/2}. The spectra for the reduced samples are shown in Fig. 4.

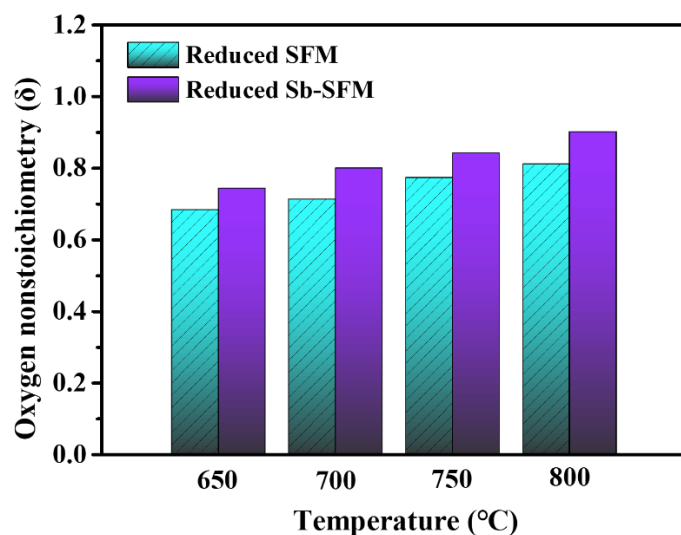


Fig. S6 Oxygen nonstoichiometry (δ) for reduced SFM ($\text{Sr}_2\text{Fe}_{1.5}\text{Mo}_{0.5}\text{O}_{6-\delta}$) and Sb-SFM ($\text{Sr}_2\text{Fe}_{1.5}\text{Mo}_{0.4}\text{Sb}_{0.1}\text{O}_{6-\delta}$) at 650, 700, 750 and 800 °C, respectively. The values are calculated from the TG and XPS results.

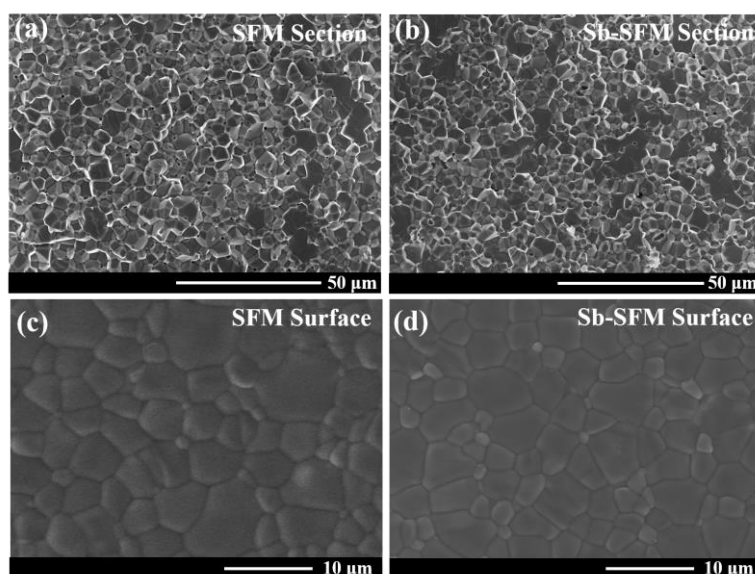


Fig. S7 SEM analysis for SFM and Sb-SFM bars sintered in air at 1350 °C for 5 h. Cross-sectional images for (a) SFM and (b) Sb-SFM, and surface images for (c) SFM and (d) Sb-SFM. Their densities exceed 97% as determined with Archimedes method. And the two samples have very similar microstructures.

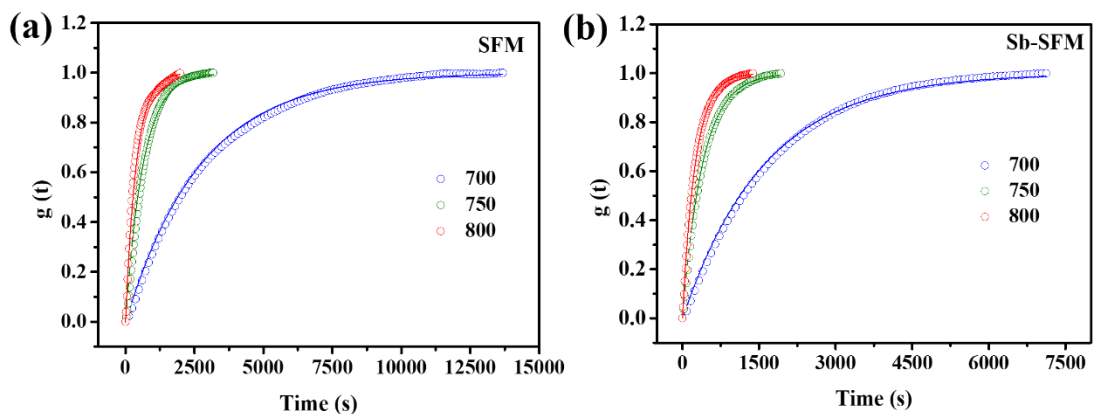


Fig. S8 Normalized conductivity and ECR fitting results for (a) SFM and (b) Sb-SFM bar samples. The measurement was conducted by increasing the hydrogen partial pressure from 5% H₂/Ar to 10% H₂/Ar for hydrogen oxidation reaction.

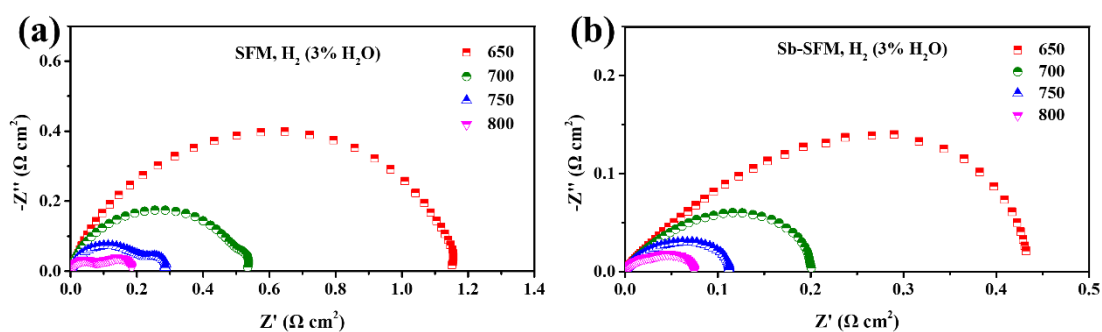


Fig. S9 Electrochemical impedance spectra (EIS) of symmetric cells supported on LSGM electrolytes measured in humidified H₂ from 650 to 800 °C: (a) SFM electrodes, (b) Sb-SFM electrodes. The ohmic resistance, which is generated from the electrolytes and the wires, has been zeroed in order to better compare the performance of the electrodes.

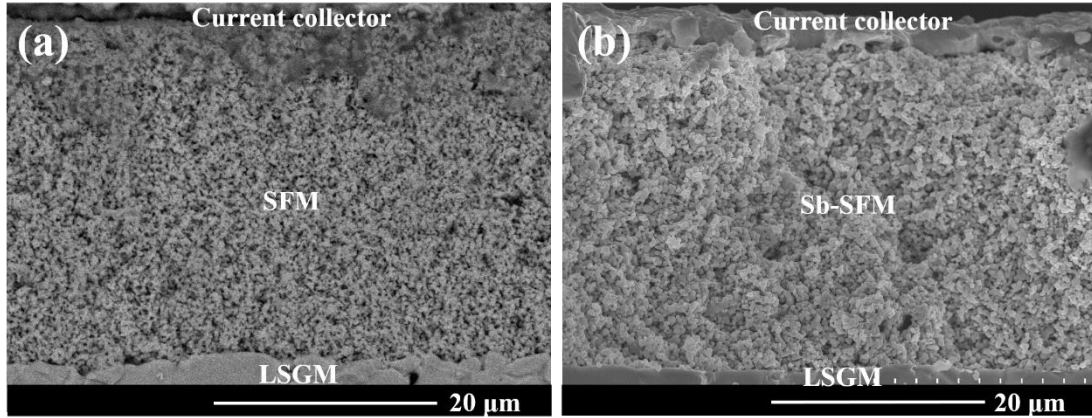


Fig. S10 SEM cross-sectional images of symmetrical cells with (a) SFM electrode and (b) Sb-SFM electrode. The SFM and Sb-SFM electrodes have similar structures and are both in good contact with the dense LSGM electrolytes.

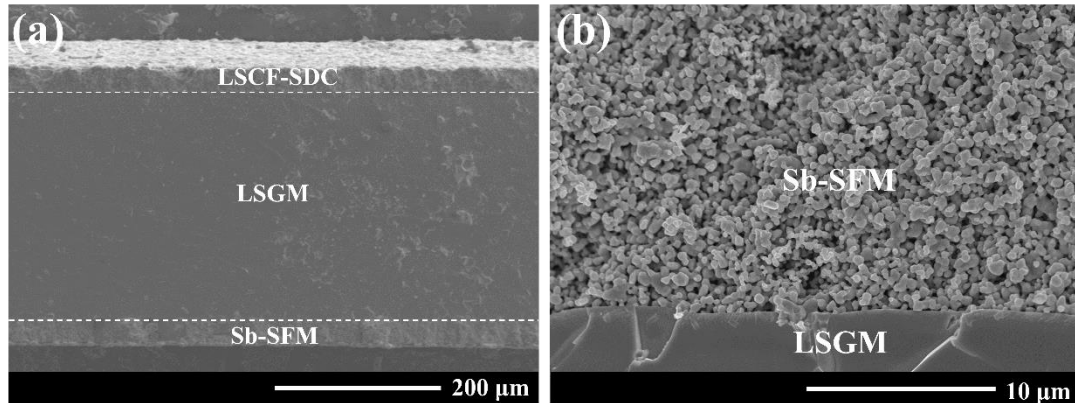


Fig. S11 SEM cross-sectional images after the durability test for 220 h using humidified H_2 as the fuel: (a) whole single cell showing the three-layer structure of Sb-SFM/LSGM/LSCF-SDC, and (b) Sb-SFM anode showing the anode/electrolyte interface. It can be observed that the Sb-SFM anode shows good contact with LSGM electrolyte and maintains uniform pore structure, indicating that Sb-SFM materials are very stable under the SOFC operating conditions.

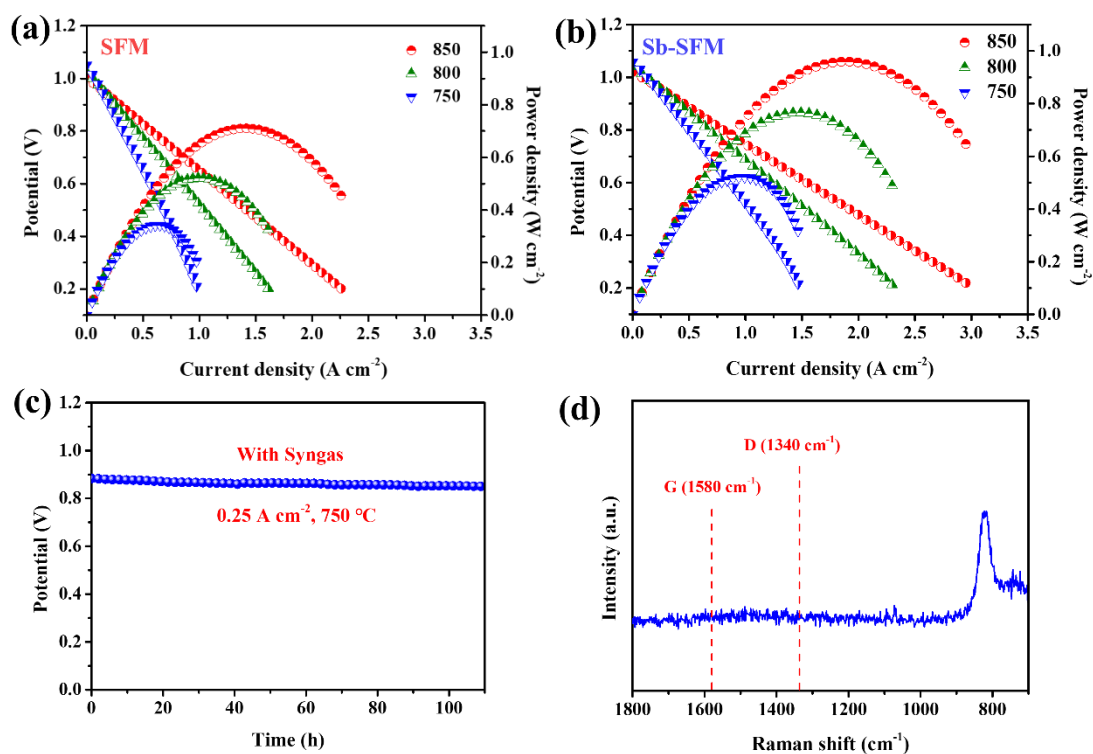


Fig. S12 Electrochemical performance of single cells supported on LSGM (280 μm) electrolytes using syngas as the fuel with (a) SFM and (b) Sb-SFM anodes, (c) the stability test for Sb-SFM anode operated at 750 $^{\circ}\text{C}$ under a current density of 0.25 A cm^{-2} , (d) Raman spectrum for Sb-SFM anode after the durability test. Neither D (1340 cm^{-1}) nor G (1580 cm^{-1}) carbon peaks can be seen, indicating no carbon is formed and deposited on the surface of Sb-SFM anode after running in syngas.

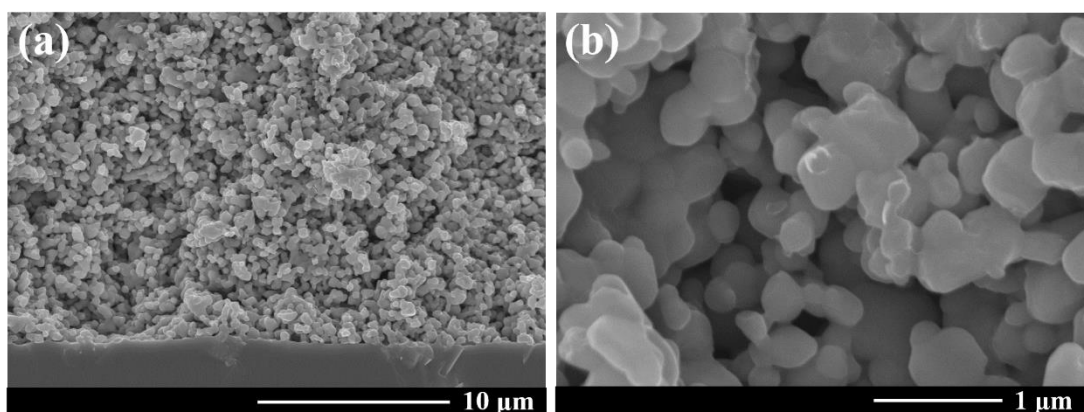


Fig. S13 SEM cross-sectional images after durability test using syngas as the fuel: (a) Sb-SFM/LSGM interface, and (b) the magnified Sb-SFM anode microstructure. It can be observed that the Sb-SFM anode shows good contact with LSGM electrolyte, indicating that Sb-SFM material is very stable under the SOFC operating conditions with syngas as the fuel.

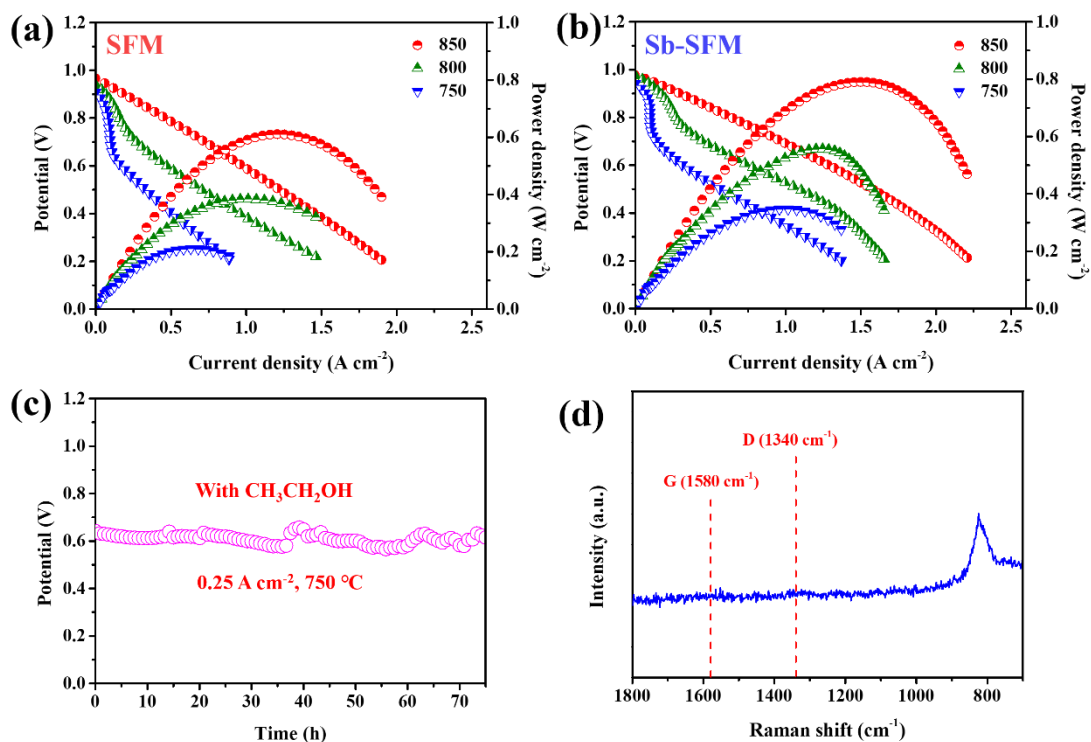


Fig. S14 Electrochemical performance of single cells supported on LSGM (280 μm) electrolytes using ethanol as the fuel with (a) SFM and (b) Sb-SFM anodes, (c) the stability test for Sb-SFM anode operated at 750 $^{\circ}\text{C}$ under a current density of 0.25 A cm^{-2} ; (d) Raman spectrum for Sb-SFM anode after the durability test. Neither D (1340 cm^{-1}) nor G (1580 cm^{-1}) carbon peaks are detected, indicating no carbon is formed on the surface of Sb-SFM anode after running in ethanol.

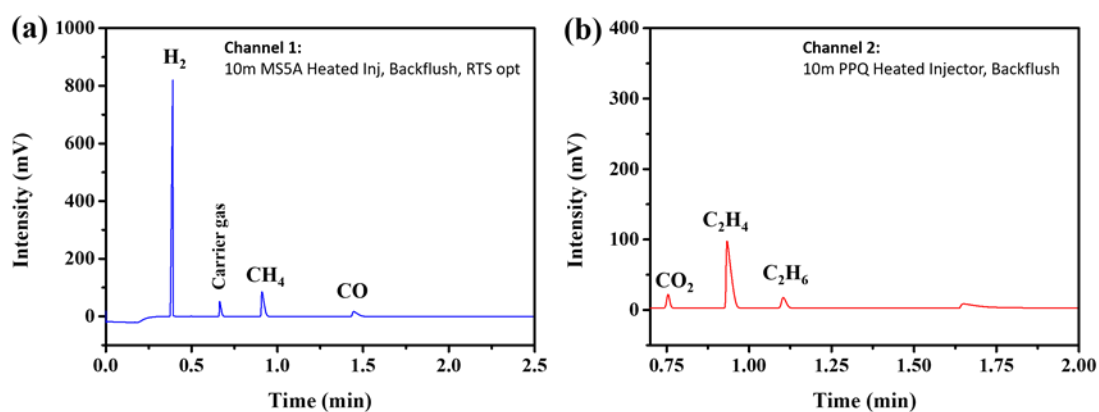


Fig. S15 The sweep gas is detected using gas chromatography with different columns when ethanol is supplied as the fuel. (a) channel 1: 10m MS5A Heated Inj, Backflush, RTS opt and (b) channel 2: 10m PPQ Heated Injector, Backflush.

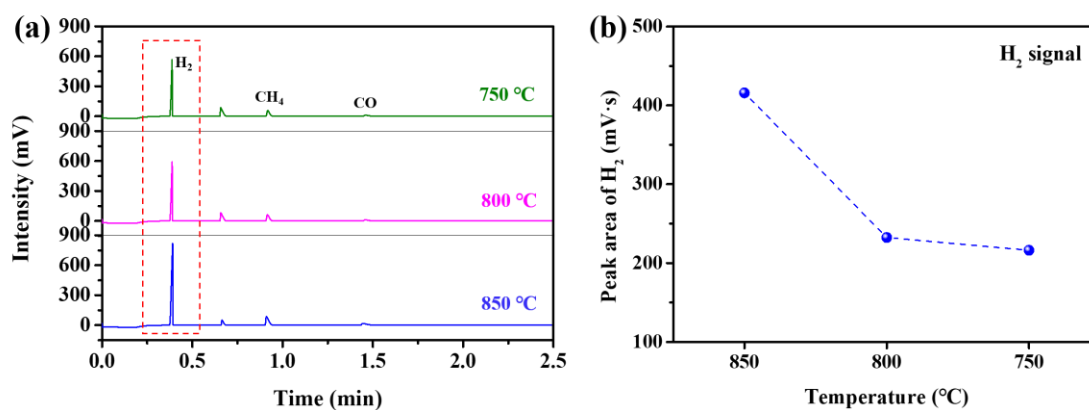


Fig. S16 Gas chromatography analysis when ethanol is supplied at OCV: (a) the sweep gas from channel 1 at different temperatures, and (b) the peak area of H₂ (corresponding to the generation of H₂) at 850, 800 and 750 °C.

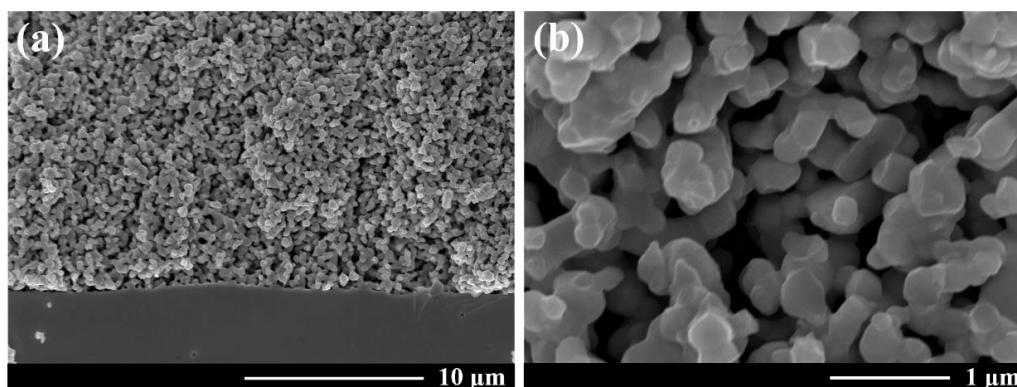


Fig. S17 SEM cross-sectional images after durability test using ethanol as the fuel: (a) Sb-SFM/LSGM interface, and (b) the magnified Sb-SFM anode microstructure. No cracking is observed between the Sb-SFM anode and the LSGM electrolyte under the SOFC operating conditions with ethanol as the fuel.

Table S1 Rietveld refinement results for the oxidized SFM and Sb-SFM.

Sample	Space group	a = b = c (Å)	V (Å ³)	R _p (%)	R _{wp} (%)	χ ²
Oxidized SFM	Pm-3m	3.917	60.098	2.40	3.37	5.84
Oxidized Sb-SFM	Pm-3m	3.912	59.868	2.07	2.76	6.54

Table S2 XPS fitting results of Fe 2p_{3/2} and Mo 3d_{5/2} for the oxidized and reduced SFM and Sb-SFM powders.

Sample	Fe ²⁺ (at.%)	Fe ³⁺ (at.%)	Fe ⁴⁺ (at.%)	Average valence of Fe	Mo ⁵⁺ (at.%)	Mo ⁶⁺ (at.%)	Average valence of Mo	δ
Oxidized SFM	15.4	51.2	33.4	3.180	26.1	73.9	5.739	0.180
Oxidized Sb-SFM	14.1	51.6	34.3	3.202	25.6	74.4	5.744	0.200
Reduced SFM	24.3	55.5	20.2	2.959	39.3	60.7	5.607	0.379
Reduced Sb-SFM	27.4	58.9	13.7	2.863	43.4	56.6	5.566	0.490

Table S3 XPS fitting results of O_{1s} for the reduced SFM and Sb-SFM samples.

Sample	B.E. O _{1s} (eV)		O _{ads} / (O _{lat} + O _{ads}) (at.%)
	O _{lat}	O _{ads}	
Reduced SFM	529.9	531.2	55.8
Reduced Sb-SFM	529.9	531.3	81.5

Table S4 EIS fitting results for SFM and Sb-SFM electrodes measured at 800 °C in humidified H₂ using symmetrical cells.

	R _H (Ω cm ²)	R _M (Ω cm ²)	R _L (Ω cm ²)
SFM	0.073	0.060	0.053
Sb-SFM	0.047	0.017	0.011